What is the Limit of Nanoparticle Strengthening?

D.C. Chrzan, J.W. Morris, Jr., Y.N. Osetsky,
R.E. Stoller, and S.J. Zinkle

Abstract

The stress required to deform a perfect crystal to its elastic limit while maintaining perfect periodicity, the so-called ideal strength, sets the gold standard for the strength of a given material. Materials this strong would be of obvious engineering importance, potentially enabling more efficient turbines for energy production, lighter materials for transportation applications, and more reliable materials for nuclear reactor applications. In practice, the strength of engineering materials is often more than two orders of magnitude less than the ideal strength due to easily activated deformation processes involving dislocations. For many materials, precipitate strengthening is a promising approach to impede dislocation motion and thereby improves strength and creep resistance. This observation begs the question: What are the limits of nanoparticle strengthening? Can the ideal strength of a matrix material be reached? To answer these questions, we need a detailed, atomic scale understanding of the interactions between dislocations and obstacles. Fortunately, simulations are beginning to explore this interaction.

Introduction

Today, the need for improved structural materials remains strong, particularly if one considers the need to develop materials well suited for energy generation. We need radiation tolerant materials for nuclear reactors; materials for turbines that can withstand higher operating temperatures; and materials for transportation that are lighter, tougher, and stronger than those presently available.

Computational hardware and theoretical advances give one hope that genuine prediction of the mechanical properties of materials is achievable. However, there are still significant barriers to be overcome. Mechanical properties of materials are often dictated not by the average structure of the material but rather by the structure and dynamics of the extended defects (e.g., dislocations, grain boundaries, and precipitates) within the material. The dynamic properties of these defects, however, are difficult to compute directly using quantum mechanics-based total-energy methods. The number of atoms necessary to do so exceeds available computational resources and will for years to come. However, the materials theory community has made progress on a number of important fronts, including predicting the structures of dislocation cores and the structures of precipitates.[1–4] In fact, modern empirical inter-atomic potentials now enable simulation of the dynamics of millions of atoms and consequently direct study of certain aspects of dislocation/precipitate interactions.

The ideal strength of a material is the stress required to strain it to its elastic limit while maintaining perfect periodicity. In 1926, Frenkel deduced that a typical metal should have an ideal shear strength on the order of one-fifth its shear modulus.[5] Because the metals of the time had strengths nearer to one one-thousandth of their shear modulus, Frenkel's estimate was puzzling. Over the next few decades, however, the existence of dislocations would be postulated as the origin of the discrepancy.[6–8] The development of electron microscopy in the 1950s made it possible to image dislocations within metals and semiconductors,[9] and since then, discussions of mechanical properties beyond the elastic limit have focused on dislocations and fracture.

Computational materials scientists, however, have begun to reconsider the importance of ideal strength calculations and have made some remarkable discoveries. For example, accurate ideal strength calculations for Mo indicate that it can yield very near its ideal strength during nanoindentation experiments.[10] At the nanoscale, a material *can* reach ideal strength.

From an engineer's perspective, ideal strength sets the absolute engineering limit for the strength of a material. It is not possible to design a microstructure that will enable a material to exceed its ideal strength. However, the fact that ideal strength can be reached at the nanoscale begs the question: Can ideal strength be reached in a bulk material?

There are at least two criteria that must be met for an engineering material to achieve a strength that approaches its ideal value.[11] First, from engineering reliability considerations, the material must be intrinsically ductile: When the material is pulled in tension, it must ultimately fail in shear, regardless of the tensile axis. Second, dislocations, if present, must be immobile at all stresses below the ideal strength.

Continuum Theory

There are a number of factors[1] that might lead to dislocation immobilization. Here, we are interested in obstacle-controlled glide where the obstacles are nanoscale precipitates embedded within the host matrix. In the usual case, the precipitate is an impediment to dislocation motion because it breaks translation symmetry. The most simple continuum model of dislocation precipitate interactions treats the obstacles as pinning points that are capable of exerting only a contact force on the dislocation, and treats the dislocation as a line of constant tension. The interaction of a dislocation with a single obstacle of this type is shown in Figure 1a. Once the dislocation contacts the obstacle, it begins to bow about it. As it bows, it exerts a force $F = 2\Gamma \cos(\varphi/2)$ on the obstacle, with Γ being the line tension of the dislocation. When the bowing angle, φ, decreases to a critical value, φ_c, corresponding to the maximum force an obstacle can withstand, the obstacle is bypassed.

A single obstacle cannot arrest the motion of a dislocation. However, a finite density of obstacles can pin a dislocation. The obstacles in most materials are

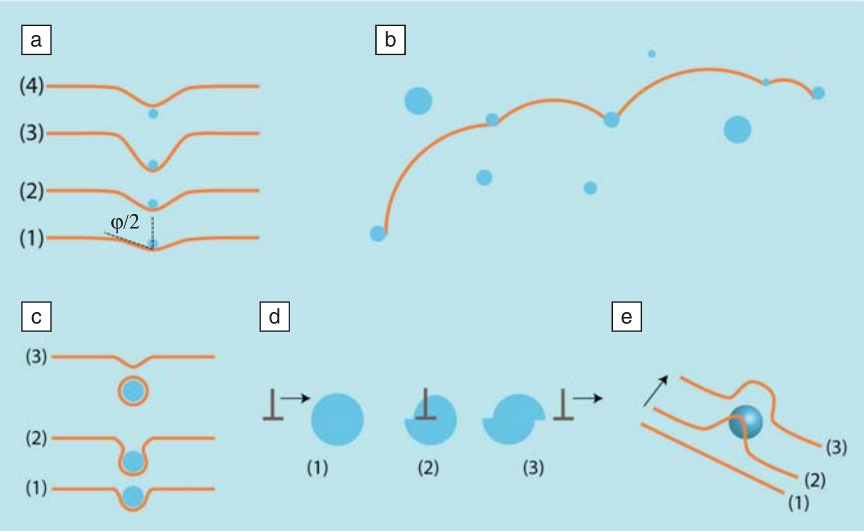

Figure 1. (a) The interaction of a dislocation with a precipitate. The bowing angle, φ, is indicated. The time sequence is numbered, with (1) indicating the earliest time. The dislocation bows about the point obstacle until φ reaches a critical value, and the dislocation unpins from the obstacle. (b) In crystals, the obstacles are arranged in an irregular pattern, and their sizes and strengths vary. (c) If one considers the obstacles to have finite size, they can be bypassed through an Orowan bowing mechanism in which a dislocation loop is left behind. Again, the sequence is numbered according to time. (d) Time sequence of the cutting of a precipitate by passage of an edge dislocation. (e) The bypass of an obstacle via dislocation climb.

arranged in a somewhat random fashion, as shown in Figure 1b, and a statistical analysis of the dislocation/precipitate interaction is required. Kocks proved that there is a critical stress (τ_c) for the passage of a dislocation through a disordered array of infinitely strong point obstacles.[12] Foreman argued that the number of defects in contact with a dislocation varies as $\tau^{-1/3}$ (τ is shear stress), and this leads to the prediction[13] that

$$\tau_c = \left(\frac{2\Gamma}{lb}\right)\left(\cos\frac{\varphi_c}{2}\right)^{3/2}, \tag{1}$$

with l defined to be the average distance between obstacles in the slip plane of the gliding dislocation with a Burgers vector of magnitude b. Later, Morris et al.[14–22] and Labusch[23] extended the theory to consider the more realistic situation of random arrays of obstacles with variable strengths and sizes. These effects contribute numerical corrections to the critical stress for sustained motion of a dislocation, which now is given by:

$$\tau_c = \alpha\beta_c^{3/2}\left[\frac{2\Gamma}{lb}\right], \tag{2}$$

with α being a numerical factor reflecting the geometric arrangement of obstacles (approximately equal to 0.9 for randomly distributed obstacles) and β_c being the dimensionless strength of the obstacles. The maximum resistance of an obstacle that is "looped" is lowered by the mutual attraction of the arms of the dislocation as they wrap around it, with the consequence that the maximum value of the obstacle strength, β_c, drops from 1.0 in the point obstacle model to about 0.7 in the multiple obstacle model, depending on obstacle sizes and configuration.[24]

It is worthwhile to compare the critical stress predicted by Equation 2 to the ideal shear strength of the material. Typically, the ideal shear strength of a material scales with the shear modulus (G) according to $\tau_{\text{ideal}} = \eta G$, with η being a constant of the order 0.1. Equating the ideal shear strength to the critical stress for dislocation motion yields the average obstacle spacing, l_c, required to pin dislocations at the ideal shear strength:

$$l_c = \frac{\alpha\beta_c^{3/2}}{\eta}\frac{K}{G}b, \tag{3}$$

with K being the dislocation energy coefficient. For an elastically isotropic material, $l_c \approx 5b$, a spacing that corresponds to a very high density of obstacles.

Experimental Background

The most detailed experimental understanding of dislocation/defect interactions comes through the study of simple, model alloys. Al-Sc alloys are a convenient system for the exploration of the dislocation/precipitate interactions. Through aging experiments, one can precipitate Al_3Sc particles and control their size and spacing.[25] Further, the temperatures required for coarsening exceed those necessary to observe dislocation mediated creep, so both constant strain rate and creep tests can be conducted on alloys with constant microstructure.

Consider dislocation motion under constant strain rate conditions. For small precipitates, on the order of 1.4 nm in diameter, dislocations bypass the precipitates during constant strain rate experiments by cutting through them. Interestingly, one piece of evidence for this stems from the different structure of dislocations in the Al matrix and the $L1_2$ ordered Al_3Sc precipitates. Both the $L1_2$ phase and the matrix phase are cubic. However, the Burgers vector of the $L1_2$ phase is twice as long as that for the matrix phase. The net result is that passage of a single dislocation through the precipitate is accompanied by the production of an antiphase boundary. The passage of a second dislocation eliminates the boundary, and this leads to a binding of the dislocations within the precipitate (Figure 2a). Observation of this pinning in post-deformation transmission electron microscopy (TEM) experiments is proof that dislocations cut small precipitates.[25] Similar observations suggest precipitate cutting in other materials.[26,27]

For longer aging times, the precipitates increase in size. Concomitantly, the larger spacing between obstacles enables their bypass through Orowan bowing. This behavior is observed in Al-Sc for average particle sizes of 5.9 nm (Figure 2b). For Orowan bypass and precipitate cutting mechanisms, the predicted yield strength enhancements are in good agreement with the predictions of simple theories.[25]

Creep experiments are also insightful. There is a threshold stress below which the steady state strain rate vanishes. In a cursory analysis of creep experiments, this threshold stress appears as a large stress exponent for the steady state creep rate. The existence of a threshold stress is, in fact, what one expects for precipitate strengthening. However, in the case of Al-Sc alloys, this threshold stress is well below the stress expected from interparticle spacings and Orowan bowing. The reason for this is quite simple: under creep conditions, the dislocations are able to climb in order to avoid interactions with obstacles (Figure 1e). The dislocations thus exploit thermally activated, stress-driven, nonconservative processes to bypass obstacles.

Performing straining experiments within a TEM provides, perhaps, the most direct information regarding dislocation–defect interactions. *In situ* experiments have been conducted in Fe-Cu alloys,[28–31] Al alloys,[32–34] and on irradiated or quenched fcc metals[35–37] and have been used to measure the average distance between pinning points within a single dislocation, as well as to estimate the strengths of obstacles.

Nogiwa et al.[28,29] have studied the interaction of dislocations and precipitates in Fe–Cu alloys. They used the observed bowing angles at unpinning to estimate the strength of precipitates less than 4 nm in diameter. They found that on average, for their Fe–1.0 wt% Cu alloy aged 20 minutes at 525°C, a screw dislocation with an average obstacle spacing of 111 nm unpins when $\cos(\varphi_c/2) = 0.22$. Using the model of Foreman and Makin,[13,38] they deduced that the yield strength of their alloy should have increased by 76 MPa relative to the sample that was not aged. The experimentally observed increase was 70 MPa, yielding very satisfactory agreement.

Atomic Scale Modeling of Dislocation/Nanoparticle Interactions

Experiments described in the previous section provide ample incentive to construct atomic scale models of dislocation–precipitate interactions, and the development of such simulations is proceeding rapidly. In developing these simulations, a number of factors must be considered. First, the stress and strain fields associated with dislocations are long-ranged. Consequently, the applied boundary conditions are an important aspect of the problem. Second, the study of dynamics must be conducted with care. Molecular dynamics simulations are capable of following dynamics over time periods on the order of nanoseconds. Experimentally, dislocation-based plasticity can evolve over hours, days, and even years. Extrapolating over time spans this large is not trivial.

A model developed in Reference 39 resolves some of the problems mentioned previously. In this model, a crystal containing an initially straight infinite edge dislocation is simulated. Periodic boundary conditions are applied along the initial dislocation line direction and the direction of the Burgers vector. This configuration places a net bending stress on the supercell used in the calculation. The effects of this bending stress are minimized by placing the dislocation on the central glide plane of the unit cell along the bending neutral axis. The model enables the study of motion over significant distances and a range of obstacle densities, sizes, and system temperatures.

Fe–Cu alloys form a prototypical system for atomic scale study using empirical potentials.[40,41] The Cu in these alloys initially precipitates within the bcc phase, and small particles are coherent with the Fe lattice. As particle sizes increase, the particles transform to a 9R and then to a 3R structure, which are commonly observed at low temperatures in some materials that are bcc at room temperature.[30] The 9R structure can be thought of as an fcc structure with a stacking fault every third plane so that its stacking sequence is ABCBCACABABC; the 3R structure is a bit more complicated. Though a number of important observations emerged from simulations of this material,[42,43] here we focus on a subset of the conclusions.

Atomic scale simulations enable direct measurement of φ_c. The critical stress and bowing angles observed in atomic scale simulations indicate that the simple line tension model overestimates the strength of the array. At higher bowing angles, the elastic attraction between dislocation segments attached to the precipitate becomes substantial (Figure 3) and assists the dislocation in bowing through the obstacle array.

Atomic scale simulations also allow one to assess more directly the importance of precipitate size. A continuum theory for a periodic array of obstacles reflecting dislocation self stress predicts:

$$\tau_c \frac{l}{Gb} = \frac{1}{2\pi}\left(B + \ln\left[\frac{dl}{bl + bd}\right]\right), \tag{4}$$

where G is the shear modulus, d the diameter of the obstacles, l the distance

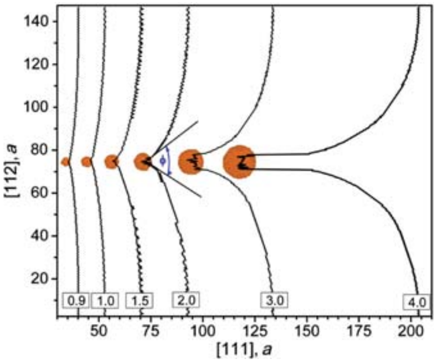

Figure 3. Dislocation configurations at the critical bypass stress as predicted by atomic scale simulations.[42] The initial edge dislocations are in α-Fe and are interacting with Cu precipitates. The lines correspond to the positions of the dislocation cores, and the results of several calculations are shown. The size of the precipitate (in nm) labels each configuration, and the bowing angle is indicated. For small precipitates, the obstacles are bypassed by cutting. At larger precipitate sizes, cutting is still predominant, but the dislocation bowing angle decreases to zero, allowing dislocation self-interactions to approach those associated with Orowan bowing.

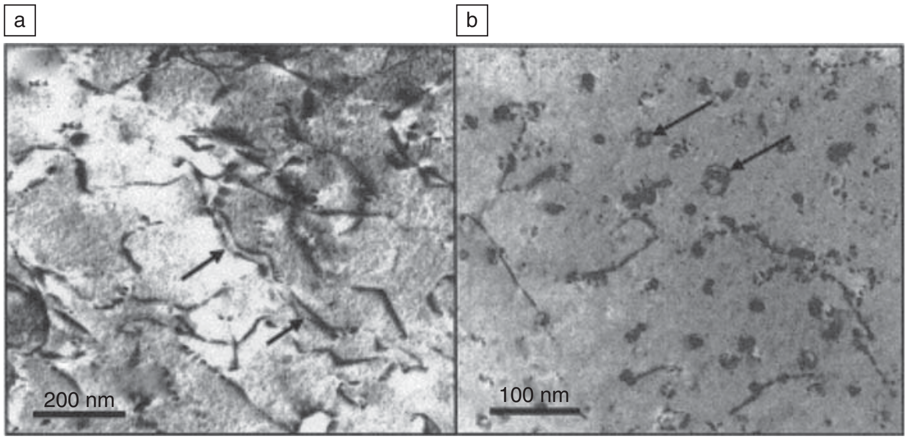

Figure 2. Dislocations interacting with precipitates in an Al–Sc alloy. (a) The arrows point to dislocations that have become paired within Al_3Sc precipitates. The precipitates in this alloy are approximately 1.4 nm in diameter. (b) Dislocation loops surrounding precipitates. The precipitates in this alloy are, on average, 5.9 nm in diameter. The loops (indicated by arrows) are strong evidence of Orowan bowing, as shown in Figure 1c. Images from Reference 25. Reprinted with permission. © 2002, Elsevier.

between obstacle edges, and *B* a constant reflecting the atomic scale properties of the obstacles.[24] (For impenetrable obstacles, $B \approx 0.7$; for voids, $B \approx 1.52$.) Figure 4 plots the critical stress for obstacle bypass obtained from the simulations[42] as suggested by Equation 4. Though the relationship determined from atomic scale simulations is linear, Equation 4 underestimates the slope of the line by a factor of two (or so) and overestimates the value of *B* substantially.

Examination of the atomic scale simulations reveals a possible origin of the deviation. Precipitate cutting dominates at all precipitate sizes. However, for larger precipitates, the critical bowing angle approaches $\varphi_c = 0$, and the dislocation passing through the precipitate leaves behind both interstitials and vacancies. Thus the bypass mechanism depends on size, and the strength of the precipitates increases more rapidly with diameter than expected from the continuum model.

Atomic scale simulations in this system also have suggested another interesting mechanism for precipitate strengthening in these alloys. The dislocation core structure within the precipitate differs from that in the matrix, and this allows another type of interaction between the dislocation and the precipitate:[44,45] a reduction of dislocation core energy when within the precipitate. This strengthening effect is estimated to be substantial, leading to strength enhancements on the order of 350 MPa for the configurations studied.[45]

Recently, more detailed studies of the interaction of screw dislocations with Cu precipitates have been conducted. Shim et al.[43] simulated a screw dislocation driven to bypass an initially bcc Cu precipitate in Fe. They observed that screw dislocations can induce a martensitic phase transformation within the precipitate (Figure 5). Specifically, for precipitates with a diameter of 2.5 nm and an applied stress of 1 GPa, when the dislocation first makes contact with the precipitate, the internal structure of the precipitate changes: Some atoms have a local coordination expected for hcp and, to a lesser extent, for fcc lattices. As the interaction continues, the extent of the transformation spreads, reaches a maximum, and then begins to decline as the dislocation bypasses the obstacle through an Orowan looping mechanism. The transition appears to be driven by the large dislocation and applied stresses. Its observation, even only as a transient effect, is compelling evidence that dislocations can alter the internal structure of precipitates, as suggested by multiple analyses.[30,43,46] This transformation is not observed for edge dislocations, which typically cut precipitates of this size in similar simulations. Shim et al.[43] conclude that the transformation of the precipitate increases its resistance to cutting. In more general terms, the internal structure of the nanoprecipitate can make a substantial contribution to its strength.

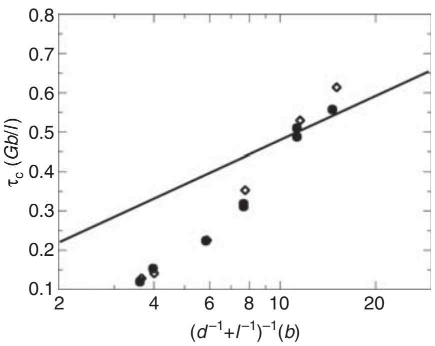

Figure 4. Dependence of critical stress for obstacle bypass on the size and separation of obstacles.[42] The line is the prediction of Reference 24. Symbols are the results for precipitate/dislocation interactions.[42] The diameter of the obstacles is given by *d*, *G* is the shear modulus, *b* is the magnitude of the Burgers vector, and *l* is the spacing between obstacles.

Atomistic-calculation based estimates of the critical stress for edge dislocation motion in the Fe-Cu system vary substantially. Nedelcu et al. estimated that for precipitates approximately 3 nm in diameter with a density of one every 7 nm, the critical stress for dislocation passage is approximately 5.1 GPa,[47] an appreciable fraction of the ideal shear strength of Fe computed using density functional theory, 7–8 GPa.[48] More recent analyses, however, suggest a smaller critical stress for the same problem.[42] Clearly, more research is needed to resolve this discrepancy and to establish reliable methods for estimating critical stresses for dislocation passage.

Conclusions

Given these observations, we now can return to the question posed in the title of this article. As noted in the discussion of Equation 3, the density of obstacles required to pin a dislocation at the ideal shear strength for an elastically isotropic material is very high. So high, in fact, that ideal strength is probably not accessible via precipitate strengthening, regardless of the strength of the precipitates. However, Equation 3 still leaves at least one avenue by which ideal strength might be reached through precipitate strengthening. Most materials are *not* elastically isotropic, and consequently, $K/G \neq 1$. Hence a material's susceptibility to precipitate strengthening depends on its elastic constants. Further, if one can increase substantially the value of *K/G*, one may be able to reach ideal strength through precipitate strengthening.

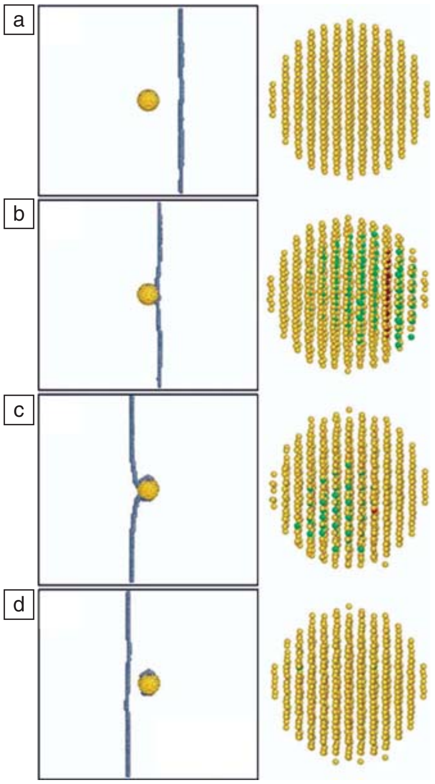

Figure 5. A screw dislocation in Fe interacting with a 2.5-nm diameter Cu precipitate.[43] The frames (a)–(d) show successive configurations in time for a dislocation driven by a stress of 1 GPa. Yellow atoms are (locally) bcc, red are fcc, and green are hcp. The precipitate transforms while the dislocation is interacting with the precipitate, and then it transforms back to the bcc structure.

Toyota Research recently introduced a class of Ti–Nb-based alloys it refers to as "Gum Metal."[49] These alloys have a number of interesting properties: high yield strength on the order of 1.2 GPa, an elastic limit of 2.7% strain, and 10% elongation with no noticeable work hardening. Further, TEM examination of the post-deformation microstructure did not reveal the presence of obvious dislocations but instead identified large planar faults, an observation that led Saito et al. to suggest that Gum Metals are deforming at or near their ideal strength.[49]

The possibility that Gum Metals are deforming at or near their ideal strength is intriguing. In designing Gum Metal, the goal was to modify the material to the point where $C_{11} - C_{12} \approx 0$, with C_{11} and C_{12} being two of the elastic stiffness constants for a cubic material. Under these circumstances, the (on average) bcc lattice of Gum Metal becomes unstable with respect to an (on average) hcp structure. Interestingly, an anisotropic elasticity theory analysis of the ratio K/G for the predominant slip systems in the bcc alloy shows that $K/G \to \infty$ as $C_{11} - C_{12} \to 0$.[11] Gum Metals were designed, in effect, to have dislocations easily pinned by obstacles and are thus exceptional candidates for nanoparticle strengthening, perhaps even to very near their ideal limit.

Thus the limit of precipitate strengthening is determined by both the strength of the nanoscale precipitates *and* the linear elastic properties of the matrix. Both of these aspects of the problem can be addressed directly using modern computational methods, and one can now explore, in detail, the limits of nanoparticle strengthening.

Acknowledgments

DCC and JWM acknowledge the support of the National Science Foundation under Grant No. DMR-0706554. YNO, RES, and SJZ acknowledge the support of the Division of Materials Sciences and Engineering and the Office of Fusion Energy Sciences, U.S. Department of Energy, under contract DE-AC05-000R22725 with UT-Battelle, LLC.

References

1. V. Vitek, *Prog. Mater. Sci*. **36**, 1 (1992).
2. X. Xu, S.P. Beckman, P. Specht, E.R. Weber, D.C. Chrzan, R.P. Erni, I. Arslan, N. Browning, A. Bleloch, C. Kisielowski, *Phys. Rev. Lett*. **95** (2005).
3. D.R. Trinkle, C. Woodward, *Science* **311**, 177 (2006).
4. E.A. Marquis, D.N. Seidman, M. Asta, C. Woodward, V. Ozolins, *Phys. Rev. Lett*. **91** (2003).
5. J. Frenkel, *Z. Angew. Phys*. **37**, 572 (1926).
6. M. Polyani, *Z. Phys. A: Hadrons Nucl*. **89**, 660 (1934).
7. E. Orowan, *Z. Phys. A: Hadrons Nucl*. **89**, 605 (1934).
8. G.I. Taylor, *Proc. R. Soc. London, Ser. A* **145**, 362 (1934).
9. W.C. Dash, *J. Appl. Phys*. **30**, 459 (1959).
10. C.R. Krenn, D. Roundy, M.L. Cohen, D.C. Chrzan, J.W. Morris, *Phys. Rev. B* **65** (2002).
11. T. Li, J.W. Morris, N. Nagasako, S. Kuramoto, D.C. Chrzan, *Phys. Rev. Lett*. **98** (2007).
12. U.F. Kocks, *Philos. Mag*. **13**, 541 (1966).
13. A.J.E. Foreman, M.J. Makin, *Philos. Mag*. **14**, 911 (1966).
14. S. Altintas, K. Hanson, J.W. Morris, *J. Eng. Mater. Technol., Trans. ASME* **98**, 86 (1976).
15. S. Altintas, J.W. Morris, *JOM* **27**, A28 (1975).
16. S. Altintas, J.W. Morris, *Acta Metall*. **34**, 801 (1986).
17. S. Altintas, J.W. Morris, *Acta Metall*. **34**, 809 (1986).
18. K. Hanson, J.W. Morris, *J. Appl. Phys*. **49**, 3266 (1978).
19. K. Hanson, J.W. Morris, *J. Appl. Phys*. **46**, 2378 (1975).
20. K. Hanson, J.W. Morris, *J. Appl. Phys*. **46**, 983 (1975).
21. J. Glazer, J.W. Morris, *Philos. Mag. A* **56**, 507 (1987).
22. J. Glazer, J.W. Morris, *Acta Metall*. **36**, 907 (1988).
23. R. Labusch, *J. Appl. Phys*. **48**, 4550 (1977).
24. D.J. Bacon, U.F. Kocks, R.O. Scatterg, *Philos. Mag*. **28**, 1241 (1973).
25. D.N. Seidman, E.A. Marquis, D.C. Dunand, *Acta Mater*. **50**, 4021 (2002).
26. W. Liu, T. Pretorius, H. Rosner, D. Ronnpagel, E. Nembach, *Mater. Sci. Eng., A* **234**, 687 (1997).
27. B.Q. Li, F.E. Wawner, *Aluminium Alloys: Their Physical and Mechanical Properties, Pts 1–3* **331–33**, 1359 (2000).
28. K. Nogiwa, N. Nita, H. Matsui, *J. Nucl. Mater*. **367**, 392 (2007).
29. K. Nogiwa, T. Yamamoto, K. Fukumoto, H. Matsui, Y. Nagai, K. Yubuta, M. Hasegawa, *J. Nucl. Mater*. **307**, 946 (2002).
30. P.J. Othen, M.L. Jenkins, G.D.W. Smith, *Philos. Mag. A* **70**, 1 (1994).
31. S. Lozano-Perez, M.L. Jenkins, J.M. Titchmarsh, *Philos. Mag. Lett*. **86**, 367 (2006).
32. B.G. Clark, I.M. Robertson, L.M. Dougherty, D.C. Ahn, P. Sofronis, *J. Mater. Res*. **20**, 1792 (2005).
33. M. Vivas, P. Lours, C. Levaillant, A. Couret, M.J. Casanove, A. Coujou, *Aluminium Alloys: Their Physical and Mechanical Properties, Pts 1–3* **217**, 1305 (1996).
34. F. Delmas, M.J. Casanove, A. Couret, A. Coujou, *Aluminum Alloys 2002: Their Physical and Mechanical Properties Pts 1–3* **396–4**, 1109 (2002).
35. R. Schaublin, Z. Yao, P. Spatig, M. Victoria, *Mater. Sci. Eng., A* **400**, 251 (2005).
36. J.S. Robach, I.M. Robertson, B.D. Wirth, A. Arsenlis, *Philos. Mag*. **83**, 955 (2003).
37. Y. Matsukawa, S.J. Zinkle, *J. Nucl. Mater*. **329–33**, 919 (2004).
38. A.J.E. Foreman, M.J. Makin, *Can. J. Phys*. **45**, 511 (1967).
39. Y.N. Osetsky, D.J. Bacon, *Modell. Simul. Mater. Sci. Eng*. **11**, 427 (2003).
40. G.J. Ackland, D.J. Bacon, A.F. Calder, T. Harry, *Philos. Mag. A* **75**, 713 (1997).
41. G.J. Ackland, G. Tichy, V. Vitek, M.W. Finnis, *Philos. Mag. A* **56**, 735 (1987).
42. Y.N. Osetsky, D.J. Bacon, *J. Nucl. Mater*. **323**, 268 (2003).
43. J.H. Shim, Y.W. Cho, S.C. Kwon, W.W. Kim, B.D. Wirth, *Appl. Phys. Lett*. **90** (2007).
44. T. Harry, D.J. Bacon, *Acta Mater*. **50**, 195 (2002).
45. T. Harry, D.J. Bacon, *Acta Mater*. **50**, 209 (2002).
46. Y.N. Osetsky, D.J. Bacon, V. Mohles, *Philos. Mag*. **83**, 3623 (2003).
47. S. Nedelcu, P. Kizler, S. Schmauder, N. Moldovan, *Modell. Simul. Mater. Sci. Eng*. **8**, 181 (2000).
48. D.M. Clatterbuck, D.C. Chrzan, J.W. Morris, *Acta Mater*. **51**, 2271 (2003).
49. T. Saito, T. Furuta, J.H. Hwang, S. Kuramoto, K. Nishino, N. Suzuki, R. Chen, A. Yamada, K. Ito, Y. Seno, T. Nonaka, H. Ikehata, N. Nagasako, C. Iwamoto, Y. Ikuhara, T. Sakuma, *Science* **300**, 464 (2003). □

Need to Connect with the Materials Research Society?

Click
www.mrs.org

Call
724.779.3003

Fax
724.779.8313

Write
506 Keystone Drive
Warrendale, PA 15086 USA
info@mrs.org

Bruker AXS

D8 DISCOVER
HRXRD
XRR
GISAXS
TEXTURE
STRESS
Jointly integrated

Superior Metrology Capability

• Advanced X-ray Solutions

- Non-destructive, non-contact metrology using X-ray technology
- Thickness, composition, crystallization phase and residual strain determination for multilayer structures
- Absolute measurements with accuracy and resolution down to atomic level – no calibration required
- Fully automated, cleanroom compatible tools for both R&D and in-line process control

www.bruker-axs.com • 1-800-234-XRAY • info@bruker-axs.com

think forward

XRD